Development of an active gust generation mechanism on a wind tunnel for wind engineering and industrial aerodynamics applications

Fred L. Haan, Jr.[†] and Partha P. Sarkar[‡]

Department of Aerospace Engineering,
Iowa State University, 2271 Howe Hall, Rm. 1200, Ames, IA 50011, USA

Nicholas J. Spencer-Berger

Dynamic Flight Loads, The Boeing Company, P.O. Box 3707 M/C: 03-KR, Seattle, WA 98124, USA

Abstract. A combination Aerodynamic/Atmospheric Boundary Layer (AABL) Wind and Gust Tunnel with a unique active gust generation capability has been developed for wind engineering and industrial aerodynamics applications. This facility is a cornerstone component of the Wind Simulation and Testing (WiST) Laboratory of the Department of Aerospace Engineering at Iowa State University (ISU). The AABL Wind and Gust tunnel is primarily a closed-circuit tunnel that can be also operated in open-return mode. It is designed to accommodate two test sections (2.44 m × 1.83 m and 2.44 m × 2.21 m) with a maximum wind speed capability of 53 m/s. The gust generator is capable of producing non-stationary gust magnitudes around 27% of the mean flow speed. This paper describes the motivation for developing this gust generator and the work related to its design and testing.

Keywords: active gust generation; non-stationary flow; wind tunnel; wind engineering.

1. Introduction

Boundary layer wind tunnels have played an integral role in the design of wind-sensitive structures for decades. Capable of simulating the lower portion of the earth's atmospheric boundary layer, these tunnels have enabled the safe design of long-span bridges, tall buildings, towers, and a host of other unique structures.

The motivation for a tunnel with advanced gusting features arose from the primary assumption in the current practice of boundary layer wind tunnel testing-that atmospheric velocity variations can be adequately modeled by stationary mean and turbulent flow properties. Extreme wind loads, however, result primarily from extreme weather events (such as gust fronts, hurricanes, etc.) where

---

† Assistant Professor, Corresponding Author, E-mail: haan@iastate.edu
‡ Professor

non-stationary gusts, transitional flow structures and rapid wind directionality changes may play a significant role. The current state-of-the-art boundary layer wind tunnels are incapable of physically simulating the transient effects of such events.

Wind tunnel simulation of the earth's atmospheric boundary layer is a well-established practice. Numerous researchers have contributed to the set of tools now in use for generating wind tunnel boundary layers that are very deep (for example, Cermak 1971, Cook 1973, Davenport 1966, Farell and Iyengar 1999). Conventional approaches employ a combination of passive devices such as spires, barrier walls, and floor roughness to generate boundary layers of the same scale as the geometric scaling of structural models placed in them. These models are then tested in a statistically stationary flow environment where the wind tunnel velocity profile, turbulence intensity profile, integral length scales and velocity spectra are matched to the scaled field values.

Passive turbulence generation techniques (such as the obstacles described previously) have been shown to produce only a limited range of possible integral scales (Bienkiewicz, *et al.* 1983). These scales are often not large enough to match prototype scales. As a result, active turbulence generation schemes have been developed to produce integral scales up to an order of magnitude larger than those of passive techniques. These techniques generally involve grids, flaps, and/or airfoils (and combinations of them) that are forced to oscillate (Bienkiewicz, *et al.* 1983, Huston 1986, Kobayashi, *et al.* 1994, Cermak, *et al.* 1995, Nishi and Miyagi 1995, Nishi, *et al.* 1999). To increase the range of turbulent flow scenarios that can be simulated, some researchers have employed arrays of individually-controlled fans as well (Kikitsu, *et al.* 1999, Nishi, *et al.* 1999).

While such devices are useful for generating a variety of turbulence scales and spectra, they have not generally been used to simulate the non-stationary gusts that can occur in hurricanes. Anemometry data from hurricanes and thunderstorms have shown that velocity records are non-stationary at times (e.g. Schroeder and Smith 1999, Orwig-Gast and Schroeder 2005). Further, while advanced analytical simulation methods for non-stationary wind fluctuations are being developed (Chen and Letchford 2005, Wang and Kareem 2005), little experimental work in this area has been attempted.

1.1. Design requirements

The goal of this project was to develop a mechanism to generate non-stationary velocity fields in the wind tunnel test sections with a capability of large magnitude velocity changes within the shortest possible time. During the design process, it was a priority to minimize the unsteady loading on the fan and any significant power fluctuation in the motor during the gust-generation operation.

A review of published full-scale data was conducted to determine the parameter value that must be achieved to generate realistic non-stationary gusts. The two primary parameters that were considered were gust magnitude and the time scale of the velocity increase. For thunderstorm-related gusts, Simiu and Scanlan (1996) summarize ranges of these parameters to involve gust magnitudes of 3 m/s to 30 m/s and gust durations from a few minutes to 20 minutes or more. Hurricane data available online are consistent with such ranges. For example, a Hurricane Andrew (Rappaport 2003) summary reported maximum sustained winds of 64 m/s with gusts up to 77 m/s (a 20% increase). Hurricane Frances data (Florida Coastal Monitoring Program 2004) showed that 3-second gusts could be 20% to 50% above the 15 minute average velocities. In a review of a number of 1995 hurricanes, Powell and Houston (1998) reported gusts from 15% to 40% above the maximum sustained wind speeds.

A wind tunnel gust generator must be able to produce comparable gusts with time scales that are realistic. Values for the rate of velocity changes were also gathered from published literature. Holmes and Oliver (2000) developed a model of the widely reported Andrews Air Force Base downburst. Their model shows a rate of velocity increase of 0.4 m/s^2 during that event. While measuring wind speeds on an instrumented tower during a weak downburst event, Sherman's (1987) data shows wind speeds changing at a rate of approximately 0.04 m/s^2. Data from a similar scenario reported by Orwig-Gast and Schroeder (2005) showed rates up to 0.25 m/s^2.

The time scales at which such events must occur will be smaller in the wind tunnel than at full scale. For example, if typical geometric scales for low to medium-rise structures, λ_L, from the wind tunnel to full scale range from 1/50 to 1/200 and a typical velocity scale, λ_V, is 1/3 to 1/2, then the time scale range would be calculated as:

$$\lambda_T = \lambda_L \Big/ \lambda_V = 0.01 \to 0.06 \qquad (1)$$

This means that full scale events that take minutes must be simulated in the wind tunnel in seconds or fractions of seconds. The scaling of the velocity accelerations, λ_A, can be found from $\lambda_A = \lambda_V / \lambda_T$. Given the velocity and time scales above, the acceleration scales could range from 5.6 to 50. In other words, the full-scale rates of velocity changes described above (0.04 m/s^2 to 0.4 m/s^2) would have to occur at rates of 0.2 m/s^2 to 20 m/s^2 in the wind tunnel. Thus a wind gust of 15-50% of the mean velocity is desirable in as little as 3 seconds with an acceleration of 0.2-20 m/s^2.

Based on these field parameters and practical limitations, it was decided to accomplish a gust of 15-25% of the mean wind speed in the wind tunnel at a rate of 0.2-10 m/s^2 in a maximum period of 5 sec. For example, the system should be able to reach a steady-state mean wind speed of 25 m/s up from 20 m/s (a 25% increase) in 5 seconds (an acceleration of 1 m/s^2). For a length scale of 1/50 and a velocity scale of 1/2, this gust would correspond to a full scale event going from 40 m/s to 50 m/s in 125 seconds (an acceleration of 0.08 m/s^2).

2. Design of the system

This section describes the details of the gust system design and the analytical tools that were developed to predict gust generation performance.

2.1. Design description

This section provides a brief description of the AABL Wind and Gust Tunnel for which this gust generation system was designed. It then summarizes the details of the bypass ducts and valves used to generate the gusts.

The wind tunnel itself became operational in October 2005 (see Fig. 1). The maximum velocity generated was 53.1 m/s (118 mph) in closed circuit mode. The wind tunnel can also operate in an open-return mode. The design includes two test sections one after the other. The *Aero* test section is located just downstream of the contraction. It has a cross section that is 2.44 m (8 ft) wide by 1.83 m (6 ft) high, and it is used for aerodynamic testing. The *ABL* test section is located approximately 15 m downstream of the *Aero* test section. Its cross section is 2.44 m (8 ft) wide by 2.21 m (7.25 ft) high, and it used to simulate atmospheric boundary layer flow. The fan is a Howden-Buffalo 108-50-710 model with 2.74 m (9 ft or 108 in.) tip-to-tip blade diameter, 1.27 m (4.2 ft or 50 in.) hub
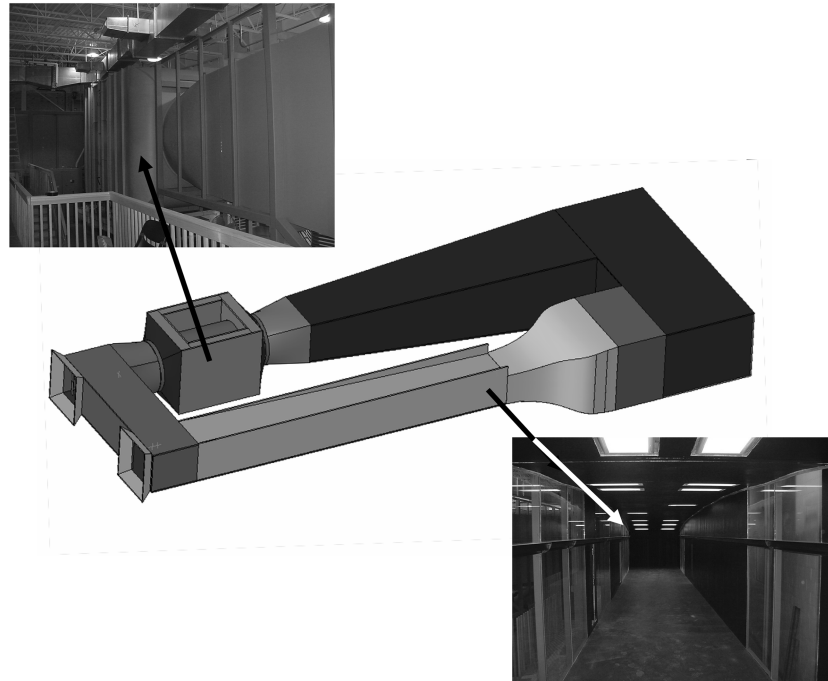
Fig. 1 Diagram of the AABL Wind and Gust Tunnel at Iowa State University. The bypass duct for the gust generator is shown in the upper left corner and the aerodynamic test section is shown in the lower right corner of this diagram

diameter and a specific flow rate of $214\,\mathrm{m^3/s}$ (452,000 cfm) generated at a static pressure of 870 Pa (3.5 in. water) and rotating speed of 710 rpm. The fan is driven by a 260 kW (350 hp) AC motor. The facility's open-return mode is configured by eliminating the sets of turning vanes at the two successive corners that follow the test sections. Both sets of turning vanes have wheels at their base to allow them to be moved into the 4.9 m (16 ft) duct that connects these corners. This duct is then isolated from the rest of the wind tunnel by two hinged doors, one at each corner. Each door forms part of one side of the corner section which becomes its perpendicular side once rotated, thereby opening the corner section to the outside and forming a U-shaped wind tunnel flow circuit.

It has been stated previously that a number of different methods of turbulence generation have been implemented by other researchers. To create the flow features, as specified in the objectives of this work, conventional means like the oscillating vanes or airfoils used in the past by others would not be practical. Changing the mean flow speed using "lossy" devices such as vanes requires the fan to operate well off of optimal conditions and induces sudden changes in electrical power requirements. Flow speed changes could also be accomplished by changing the speed of the fan-but the inertia of the fan precludes speed changes on time scales required (see previous section discussing such time scales).

The basic design that was chosen to achieve the requirements was a bypass duct. The bypass duct (conceptually similar to the transition facility described in Saric 1992) diverts flow from the main duct. This diversion reduces the flow velocity in the main test section. Computer-controlled dampers dictate the amount of flow diverted and the time scales involved. Several configurations of ducting were tested using small scale physical models. Hot wire probes were used to obtain velocity profiles
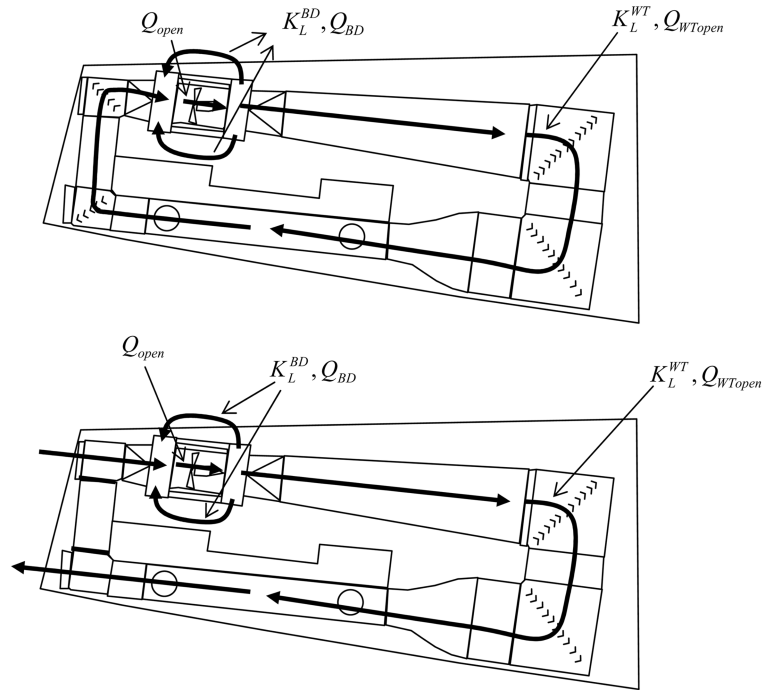
Fig. 2 Diagrams showing the wind tunnel's main circuit and bypass duct in both closed and open circuit modes. K_L^{WT} and $\tilde{K}_L^{BD}$ represent the loss coefficients through the wind tunnel test section and bypass duct circuits, respectively. Q_{BD}, Q_{WTopen} and Q_{open} are the flow rates through the bypass duct, the test section and the fan section, respectively

to determine how uniformly air could be diverted from the main duct. The final concept can be seen in the wind tunnel layout diagram shown in Fig. 2 and in the 3D and 2D illustrations of Fig. 3.

Several issues guided the design of the bypass duct. First, the amount of flow diverted through the duct had to result in a reasonable amount of velocity change in the main test section. Placed on either side of the fan section, two rectangular ducts 4.12 m (13.5 ft) high by 0.46 m (1.5 ft) wide were designed for the bypass ducts. The size of these ducts was rather seriously constrained by the building geometry. They were designed to be as large as possible given the room size. These ducts run parallel to the main duct on either side of the fan assembly and represent a bypass area of 84% of the main test section's area. Second, the bypass duct and its accompanying transition sections must minimize the amount of flow non-uniformity introduced into the main duct of the wind tunnel. This issue had two major ramifications. Removing air from the stream downstream of the fan-and upstream of the test section-may introduce large non-uniformities in the mean flow profile at the test sections that would adversely affect testing. Also, reintroducing air just upstream of the fan could inject non-uniform profiles into the fan and subject the fan to damaging unsteady periodic loading.

To address these issues-and to accommodate the building geometry-the duct transition sections were designed to take air out of and put air into the main duct evenly around its entire perimeter. The beginning and ending sections of the fan duct are circular in cross section, so this was accomplished using a 0.61 m (2 ft.) wide (axisymmetric) slot along the circumference of each of these sections. Surrounding each slot is a large plenum that acts as a transition from the slot to the
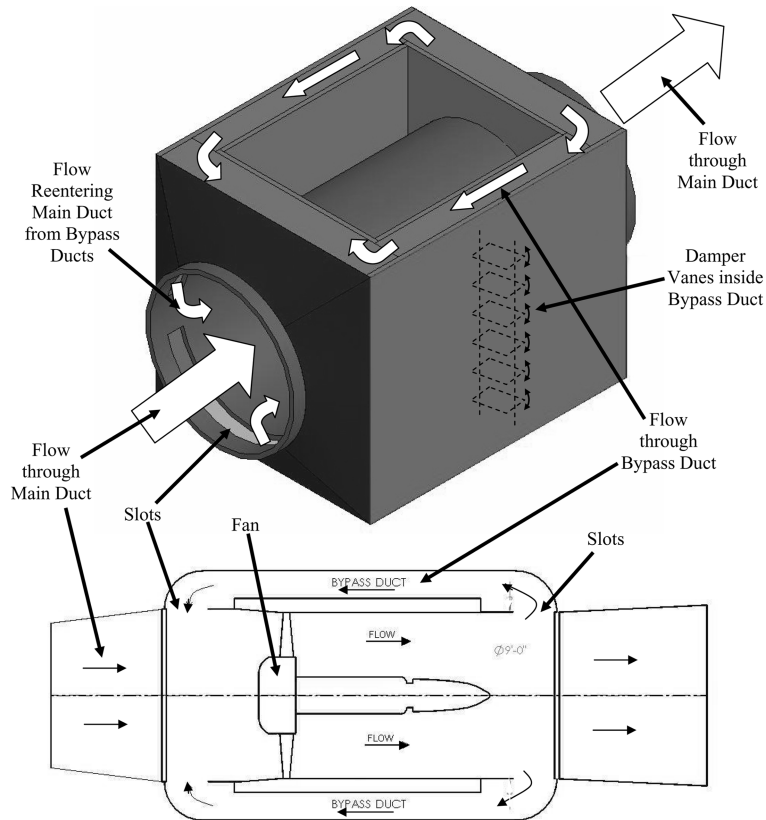
Fig. 3 Diagram of the bypass duct surrounding the portion of the main duct containing the fan. The upper diagram is a 3D illustration of the bypass ducts surrounding the fan section. The lower diagram is a top view of the system showing the fan and its relation to the bypass ducts. The slots that allow flow through the bypass duct are covered when the gusting mode is not used

bypass ducts that run on both sides of the fan. The plenum allows the flow to reorganize from the slot to the bypass duct. These slots can be completely covered (manually) to allow the wind tunnel to operate like a regular wind tunnel-as if the bypass ducts do not exist. They are only open when the gusting capability is required.

Each bypass duct is designed with a set of electromechanically controlled dampers to open and close the duct. They consist of Ruskin heavy duty, opposed-blade airfoil dampers. Each duct has 20 blades in a 46 cm by 411 cm (18 in. by 162 in.) configuration (see Fig. 3 for an illustration of the location of these dampers in the bypass ducts). The dampers can be fully open, fully closed, or fixed partially open.

2.2. Gust magnitude predictions

To predict the performance of the bypass duct concept, a set of analytical tools was derived to estimate wind tunnel test section velocity when the bypass duct was closed and when the bypass duct was open. The velocity estimates require data for the fan curve and loss coefficients to estimate the system curves. This section describes the approach first for a closed duct and then for an open duct. The section then goes on to describe how the loss coefficients were estimated for the bypass duct itself.

To predict the magnitude of the gusts that could be generated with this system, estimates had to be made of the difference in wind tunnel *Aero* test section velocity, V_{WT}, when the bypass duct was open or closed. Wind tunnel velocities (again, in the *Aero* test section) for the bypass duct open and closed are denoted here as V_{WTopen} and $V_{WTclosed}$, respectively.

To estimate the test section velocity when the bypass duct is closed, one must estimate the pressure drop through the entire tunnel circuit and use the fan curve to estimate total flow rate. To estimate the pressure drop, loss coefficients were calculated for each element of the wind tunnel-diffusers, ducts, turns, screens, etc. These loss coefficients were summed into an overall loss coefficient for the wind tunnel. This loss coefficient was then related to the pressure drop through the tunnel as:

$$\Delta p_{WTclosed} = \frac{1}{2} \rho V_{WTclosed}^2 K_L^{WT_{closed}} \qquad (2)$$

where $\Delta p_{WTclosed}$ is the pressure drop through the main test section when the bypass ducts are closed and $K_L^{WT_{closed}}$ is the loss coefficient (referenced to the *Aero* test section velocity) of the main circuit when the bypass duct is closed. One issue should be noted here. The loss coefficient, K_L^{WT}, will have three different values depending on the configuration of the wind tunnel. When the axisymmetric exit and entry slots to the bypass duct are covered, you have one loss coefficient denoted $K_L^{WT_{clean}}$. When these slots are open, you have loss coefficients of $K_L^{WT_{open}}$ and $K_L^{WT_{closed}}$ when the bypass duct dampers are open and closed, respectively. Values for each coefficient are listed in (all for the wind tunnel in closed-return mode).

The test section velocity is found by locating the intersection of the fan curve and the system curve. The flow rate a fan generates is a function of the pressure drop across the fan. This function is described by the *fan curve* provided by the fan vendor. As an example, the fan curve for the wind
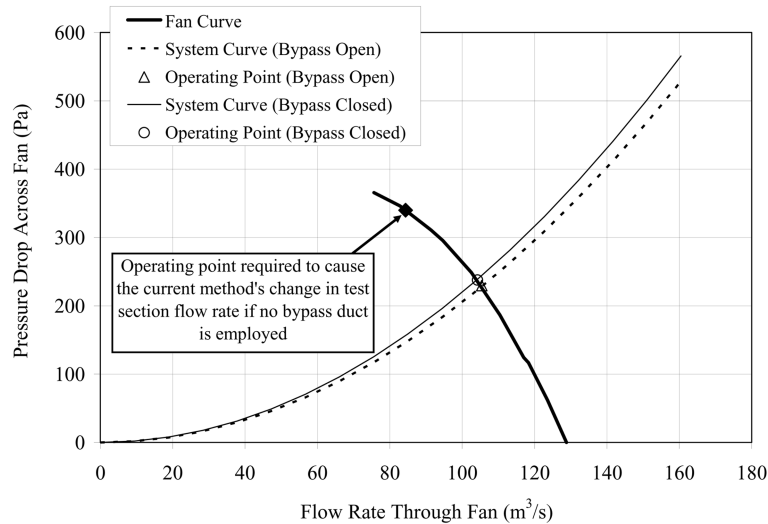

Fig. 4 Illustrative example fan curve and two system curves for the fan running at 50% full speed. The upper system curve represents the wind tunnel circuit with the bypass dampers closed and the lower system curve represents the wind tunnel circuit when the bypass dampers are open. If no bypass duct is employed, one would have to increase the pressure drop across the fan to the point indicated to achieve the current method's change in test section flow rate

tunnel fan (running at 50% full speed) is plotted in Fig. 4. The pressure drop across the fan (and also across the wind tunnel circuit) is in turn a function of the aerodynamic properties of the wind tunnel itself. Rewriting Eq. (2) in terms of the flow rate through the wind tunnel gives us the *system curve* as:

$$\Delta p_{WTclosed} = \frac{1}{2}\rho\left(\frac{Q_{closed}}{A_{WT}}\right)^2 K_L^{WT_{closed}} \tag{3}$$

where the flow rate through the wind tunnel with the bypass duct closed is Q_{closed} and A_{WT} is the cross sectional area of the *Aero* test section. A_{WT} is 4.46 m² (48 ft²). This system curve equation is also plotted in Fig. 4, and the intersection of the system curve of the wind tunnel with the fan curve of the fan corresponds to the flow rate through the circuit. With an estimate for $K_L^{WT_{closed}}$, one can use an iterative procedure to find the value of $V_{WTclosed}$ at which the fan curve and the system curve Eq. (3) intersect.

This wind tunnel will be used in two primary modes-an aerodynamic (*Aero*) testing mode and an atmospheric boundary layer (*ABL*) testing mode. In *ABL* mode, the 15.2 m (50 ft) long section between the contraction and the second test section contains passive turbulence generating obstacles. These two modes have different loss coefficients. These loss coefficients in turn depend on whether the tunnel is operated in closed-circuit or open-return mode. As part of the wind tunnel design process, $K_L^{WT_{clean}}$ values for *Aero* and *ABL* modes were estimated to be 0.64 and 0.75, respectively, for the closed-circuit operation mode. The above iterative procedure resulted in estimates of 47.7 m/s (156.5 ft/sec) and 46.2 m/s (151.7 ft/sec) for aerodynamic and *ABL* modes, respectively.

To estimate the test section velocity when the bypass duct is open, one must recognize air will flow through both the bypass duct circuit and the main circuit. The flow rates through each circuit depend on the loss coefficients and cross sectional areas of each circuit. The loss coefficients for this scenario are denoted by $K_L^{WT_{open}}$ and K_L^{BD} for the wind tunnel test section and the bypass duct, respectively. An illustration of both circuits and their loss coefficients is shown in Fig. 2. The loss coefficients quantify the pressure drop through the circuit as shown in the following equations:

$$\Delta p_{BD} = \frac{1}{2}\rho V_{BD}^2 K_L^{BD} \tag{4}$$

$$\Delta p_{WTopen} = \frac{1}{2}\rho V_{WTopen}^2 K_L^{WTopen} \tag{5}$$

where Δp_{BD} and Δp_{WTopen} are the pressure drop through the bypass duct and wind tunnel, respectively, with the bypass duct open (this is also the pressure drop across the fan) and V_{BD} and V_{WTopen} are the velocities through the bypass duct and wind tunnel (*Aero* test section), respectively, with the bypass duct open. The test section velocity, V_{WTopen}, is measured just downstream of the contraction. The pressure drop through the bypass duct circuit must equal the pressure drop through the wind tunnel circuit. Mathematically, this means that Δp_{BD} in Eq. (4) must equal Δp_{WTopen} in Eq. (5).

Eq. (4) and/or Eq. (5) could be used to generate the system curve for the open-duct configuration. As described previously and illustrated in Fig. 4, one can then estimate the flow rate through the fan by finding the intersection of the system line and the fan curve. The fan curve, in this case, will relate the total flow rate through the fan, Q_{open}, to the pressure drop across the fan. To use Eq. (5) as a system curve, one must relate the test section velocity, V_{WTopen}, to the total flow rate through the fan, Q_{open}. A derivation of this relationship follows.

Because the pressure drops around both circuits, Δp_{BD} and Δp_{WTopen}, are equal, Eqs. (4) and (5) can be combined to obtain expressions relating the velocity in the wind tunnel test section to the velocity in the bypass duct. The velocity in the bypass duct, V_{BD}, can be expressed as:

$$V_{BD} = V_{WTopen}\sqrt{\frac{K_L^{WT_{open}}}{K_L^{BD}}} \tag{6}$$

When the bypass duct is open, the total flow rate through the fan, Q_{open}, is the sum of the flow rates through the wind tunnel test section and bypass duct. One can express the total flow rate as:

$$Q_{open} = V_{WTopen}A_{WT} + V_{BD}A_{BD} \tag{7}$$

Substituting Eq. (6) into Eq. (7) allows one to derive the following expression for the flow rate through the wind tunnel test section when the bypass duct is open, Q_{WTopen}:

$$Q_{WTopen} = V_{WTopen}A_{WT} = \frac{Q_{open}}{1 + \dfrac{A_{BD}}{A_{WT}}\sqrt{\dfrac{K_L^{WT_{open}}}{K_L^{BD}}}} \tag{8}$$

Because the loss coefficients $K_L^{WT_{open}}$ and K_L^{BD} are functions of the velocities V_{WTopen} and V_{BD}, the above expressions (Eqs. (5)-(8)) can be used in an iterative procedure to locate the intersection of the fan curve and the system curve (again, see Fig. 4). This intersection provides the estimate of the fan flow rate from which the test section velocity can be calculated using Eq. (8).

These analytical tools-for both the closed and open bypass duct cases-can be used to estimate several important performance indicators. In addition to predicting the velocity differences, they can also be used to predict how much the duct open or closed will change the pressure drop across the fan and (also with the fan curve) how much more or less power will be required of the fan motor.

The loss coefficients $K_L^{WT_{closed}}$, $K_L^{WT_{open}}$ and K_L^{BD}, had to be estimated for the wind tunnel main circuit and the bypass duct circuit to use the above gust-magnitude calculation procedures. Initially, the loss coefficient for the wind tunnel main circuit in *Aero* mode with the bypass duct slots covered, $K_L^{WT_{clean}}$, was estimated to be 0.64 (using conventional procedures that are outside the scope of this paper). An estimate of 0.71 was then found for $K_L^{WT_{closed}}$ by modeling the region of the uncovered slots as a pipe junction.

$K_L^{WT_{open}}$ and K_L^{BD} had to be found simultaneously with the estimate of V_{WTopen} described above. Since both loss coefficients were dependent on the flow rates through the bypass duct and past the bypass duct entrance, they were part of the iterative procedure. With this approach the $K_L^{WT_{open}}$ value was estimated to be 1.07 using a dividing T and combining T pipe junction model. Table 1 shows

Table 1 Loss coefficients for wind tunnel test section (closed-return mode) and bypass duct circuits in different configurations

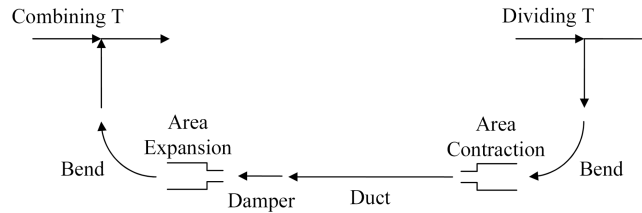|	Description	Design estimate	Measured
$K_L^{WT_{clean}}$	Slots covered	0.64	0.67
$K_L^{WT_{closed}}$	Slots uncovered, bypass duct closed	0.71	0.72
$K_L^{WT_{open}}$	Slots uncovered, bypass duct open	1.07	1.11
K_L^{BD}	Bypass duct loss coefficient	15.2	13.9

Fig. 5 Components used to model the bypass duct for the purpose of estimating loss coefficients. The loss coefficients for each component were referenced to the velocity in the bypass duct and summed to estimate the loss coefficient for this circuit

the estimated and measured values for each of these loss coefficients and the Appendix shows greater detail about these calculations. The loss coefficients for the bypass ducts, K_L^{BD}, were estimated by modeling the ducts as a series of individual components. The flow path through the bypass duct shown in Fig. 3 was modeled with the components shown in Fig. 5. These components included a dividing "T" exit flow, a bend, an area contraction, a duct flow, flow through damper vanes, an area expansion, a bend and a combining "T" entrance flow. The component loss coefficients are listed in Table 2 with the estimate of the overall bypass duct loss coefficient of 15.2. The details of this prediction in term of loss coefficient calculations for each of the components are described in the Appendix.

3. Experimental study of gust generator performance

The AABL Wind and Gust Tunnel facility became operational in October of 2005. This section reports the results of testing the bypass-duct gust generator of this facility. These results include overall performance parameters, velocity profiles in the aerodynamic test section, velocity profiles in the fan section and time dependence of the gusts. The atmospheric boundary layer mode and open-return mode of the tunnel were not tested for this project, and hence not reported here. Testing these modes is planned for the future.

Table 2 Component contributions to the loss coefficient of the bypass duct

Component	$K_{L_i}^{BD}$
1. Exit flow	16.65
2. Bend	0.87
3. Area contraction	0.33
4. Damper	1.2
5. Duct	0.05
6. Area expansion	0.42
7. Bend	0.87
8. Entrance flow	−5.20
TOTAL K_L^{BD}	15.2

Table 3 Gust generator performance when conducting a change from a bypass-duct open condition to a bypass-duct closed condition

	Velocity change	Fan pressure change	Fan power change
Design estimate	21%	4%	1%
Measured	27%	–2%	7%

3.1. Overall performance parameters

Table 3 lists comparisons between predictions made for gust generator performance parameters (described in the last section) and the values measured in the AABL Wind and Gust Tunnel. The changes being quantified are differences in test section velocity, fan pressure drop and fan motor power when one switches from having the bypass duct open to having it closed. The design estimates were made before the facility was built using the techniques described in section 2 using the original fan curve provided by the vendor. Once the facility was complete, it was found from in-situ measurements that the fan curve predicts performance somewhat below the as-built performance of the system. In situ testing found that the fan flow rate was approximately 20% greater than that predicted by the vendor's fan curve. A fan curve adjusted for this in situ performance was used to identify the measured value of K_L^{BD}. Using the measured velocity change in the test section, K_L^{BD} was found from the intersection of the fan and system curves described in the last section.

Overall, the design estimates compared very well with measurements. The increased gust magnitude is primarily due to the lower than expected bypass duct loss coefficient, K_L^{BD}. The small change in the pressure drop across the fan will minimize the unsteady loading on the fan and will minimize the pressure fluctuations due to the actuation of the dampers. This constitutes one of the *primary advantages* that this method has over conventional techniques for gust generation that involve blocking the flow with flaps or airfoils to increase tunnel loss coefficients and decrease flow rate. The bypass duct approach achieves velocity changes of 25% or more with only a 2% change in pressure drop across the fan. As illustrated in Fig. 4, generating a 25% change in flow speed in the test section merely by changing loss coefficients would require increasing the static pressure drop across the fan by nearly 40%.

3.2. Test section velocity profiles

The uniformity of the velocity profile in the test section was a priority in the design process. The goal was to produce a gust without radically changing the flow uniformity. Mean velocity and turbulence intensity profiles were measured in the AABL tunnel to determine the effect of the bypass duct on the test section flow quality.

Velocity profiles were measured using an A.A. Labs constant temperature anemometer and a straight, hot wire probe. shows the horizontal profile of mean velocity and turbulence intensity in the test section with the bypass ducts open and closed. The velocity across the test section is within 1.5% of the centerline velocity and the turbulence intensity is less than 0.15%. This same degree of uniformity and low turbulence is evident in the vertical velocity profiles of Fig. 7. Clearly, the design of the bypass duct system combined with the tunnel's flow conditioning devices (three screens and a honeycomb) is adequate to generate gusts while maintaining very uniform flow. The profiles show very little difference in turbulence intensity whether the bypass duct was open or closed. This shows
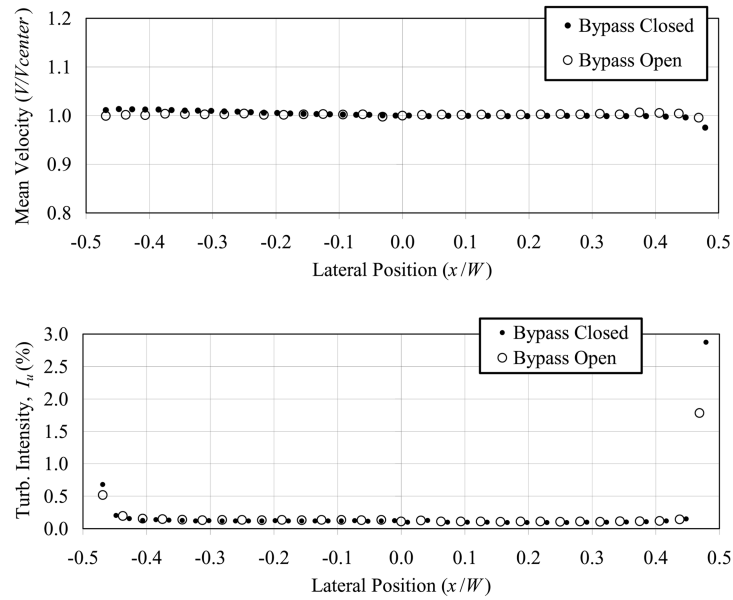
Fig. 6 Horizontal profiles of mean test section velocity and turbulence intensity for bypass open and bypass closed cases
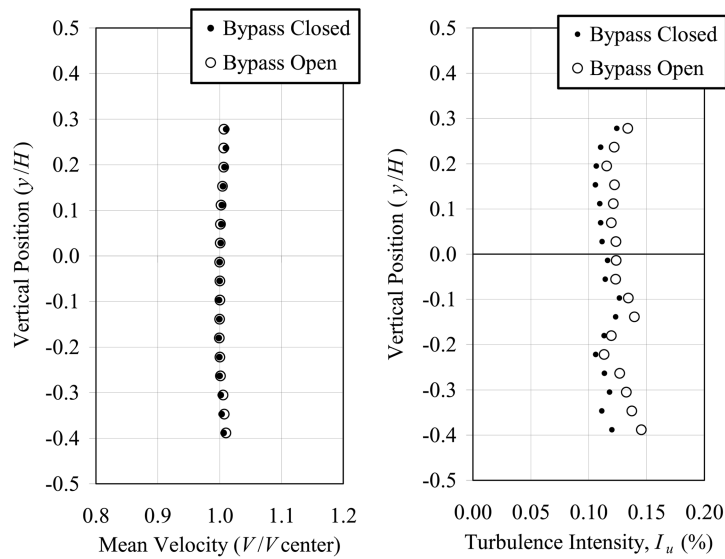

Fig. 7 Vertical profiles of mean test section velocity and turbulence intensity for bypass open and bypass closed cases

that the bypass duct system is not generating unwanted turbulence in the test section.

3.3. Fan section velocity profiles

The nature of non-uniformities ingested by the fan was quantified using an 18-hole pressure probe
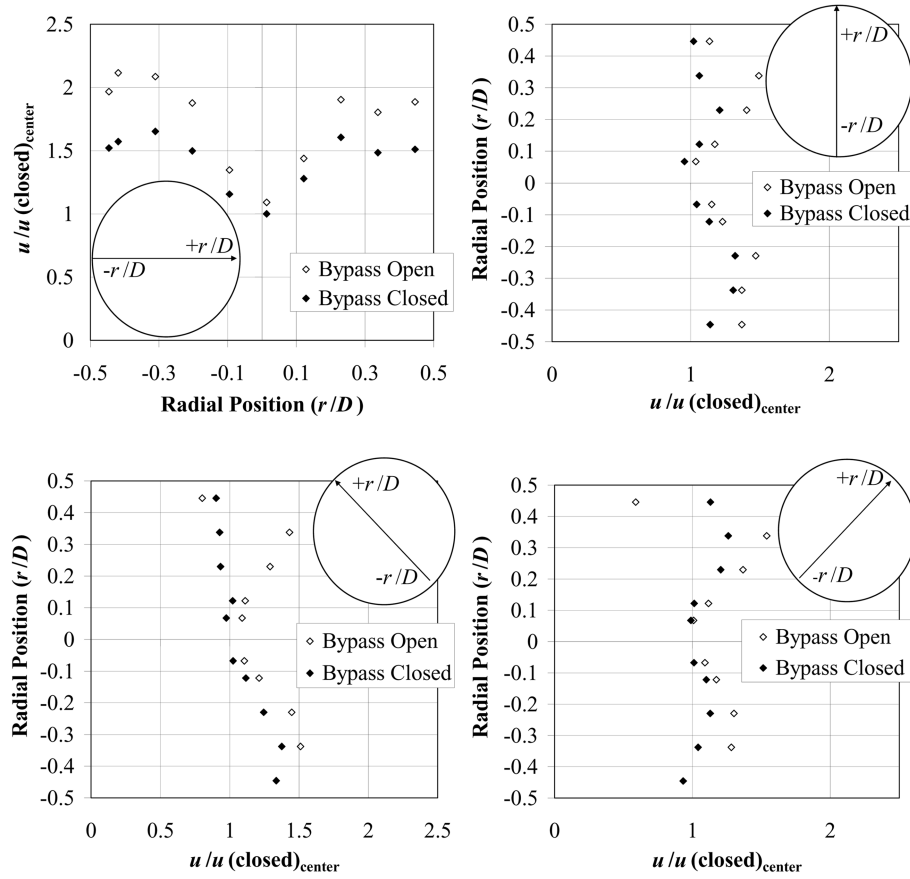
Fig. 8 Velocity profiles upstream of the fan and downstream of the reentering flow from the bypass duct

(a Dantec model PS18 Omniprobe) that could measure three components of velocity just upstream of the fan. Since the fan rotates through velocity asymmetries, it is subject to unsteady loading. The purpose of this test was to quantify any asymmetries induced by the bypass duct.

Fig. 8 shows horizontal, vertical and diagonal mean velocity profiles measured upstream of the fan and downstream of the bypass duct opening. The profiles then represent the inflow to the fan. Each profile shows low velocity near the center of the duct where the fan hub is located (hub diameter is 1.27 m). The largest asymmetry going from a bypass open to closed configuration was approximately 17%. All other bypass-induced asymmetries were less than this-many were significantly less than this. It was assumed that if the flow asymmetries generated by the bypass duct were less than that generated by a typical ABL profile (30%-60%) then the bypass performance would be deemed acceptable. The level of inflow asymmetry of the system was therefore considered acceptable.

3.4. Time dependence of gusts

A hot wire anemometer was used to quantify the time scales of the gusts in the main test section. shows a velocity time series during a ramp up gust event. In this event the damper valves in the bypass duct go from fully open to fully closed causing an increase in the test section velocity of
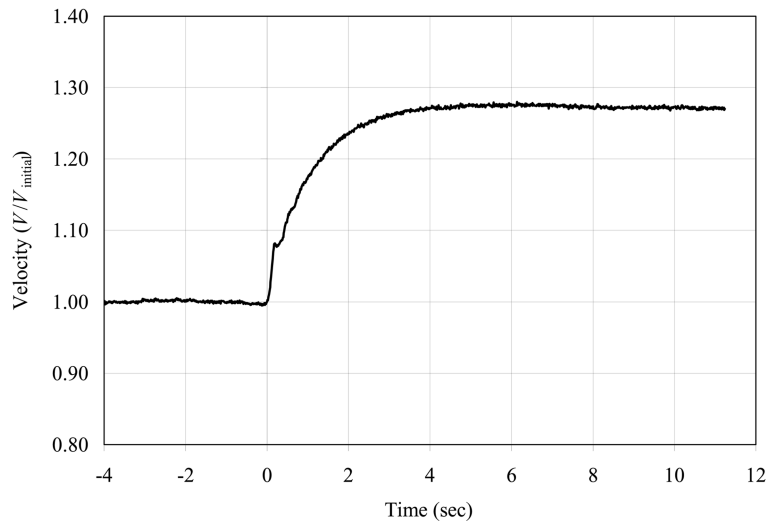
Fig. 9 Time series of test section velocity during a ramp-up gusting event. 97% of the higher-speed velocity
    is attained within 2.2 seconds.

approximately 27%. The velocity magnitude reaches 97% of the increased steady-state (or gust)
value in 2.2 seconds. In this case, the initial velocity was about 20 m/s and the final steady-state
value was 25.4 m/s. This results in a velocity acceleration value of about 2.45 m/s^2. It was observed
that this 2.2 second time interval decreases approximately linearly when the initial wind tunnel
velocity is increased. Testing the gusts with initial wind tunnel velocities from 10 m/s to 25 m/s
reduced the time interval for velocity change from 5.5 sec. to about 1 sec. The lower time interval
will result in a velocity acceleration of 5.4 m/s^2. If the velocity is increased further it is possible to
achieve the higher velocity acceleration limit of 10 m/s^2 set for the design.

   Another way to relate the gust time scale to full scale flows is to consider a gust factor versus
gust duration curves. Using a time scale, λ_T, of say 0.02 discussed previously, one finds that a wind
tunnel gust of two-second duration would be equivalent to a full scale gust duration of 100 seconds.
Marshall and Krayer's (1992) curve from Hurricane Bob gives a gust factor of approximately 1.25
for gusts of 100 seconds duration. This gust magnitude is well within the capabilities of this gust
generation system.

4. Conclusions

   A unique active gust generation mechanism for an atmospheric boundary layer wind tunnel has
been developed. A wide range of non-stationary flow structures can be simulated using a bypass
duct with flow diverted through the use of computer-controlled valves and vanes. The current
design allows for gusts between 25% and 30% of the mean flow velocity with time and velocity
acceleration scales comparable to a wide range of full scale thunderstorm and hurricane gust events.
These gust magnitudes are achieved with minimal changes in static pressure drop (2%) across the
fan where conventional techniques of using vanes or airfoils to block the flow require large static
pressure changes (up to 40% or more) to achieve similar results. These gusts are also achieved
without any significant effect on the test section velocity uniformity or turbulence level.

Future work will include investigating ways to increase the gust magnitude range. Increasing the gust magnitude range might be accomplished by adding additional damping vanes to the bypass duct and possibly the main duct. By changing the amount of blockage in one or the other duct, greater flow diversion and thus greater test section velocity change can be achieved. An obvious next step is to expose building models to these flows to investigate the effects of such gusting phenomena on aerodynamic loading.

Acknowledgements

References

Bienkiewicz, B., Cermak, J. E., Peterka, J. A., and Scanlan, R. H. (1983), "Active modeling of large-scale turbulence", *J. Wind Eng. Ind. Aerodyn.*, **13**, 465-475.

Blevins, R. D. (2003), *Applied Fluid Dynamics Handbook*, Krieger Publishing Company, Malabar, Florida.

Cermak, J. E. (1971), "Laboratory simulation of the atmospheric boundary layer", *AIAA J.*, **9**(9), 1746-1754.

Cermak, J. E., Leighton, S. C., and Leffler, R. D. (1995), "Wind-tunnel modeling of the atmospheric surface layer", *J. Wind Eng. Ind. Aerodyn.*, **54/55**, 505-513.

Chen, L. and Letchford, C. (2005), "Simulation of extreme winds from thunderstorm downbursts", *Proc. 10th America's Conference on Wind Engineering*, Baton Rouge, Louisiana.

Cook, N. J. (1973), "On simulating the lower third of the urban adiabatic boundary layer in a wind-tunnel", *Atmospheric Env.*, **7**, 691-705.

Davenport, A. G. (1966), "The treatment of wind loading on tall buildings", *Proc. Symposium On Tall Buildings*.

Farell, C. and Iyengar, A. K. S. (1999), "Experiments on the wind tunnel simulation of atmospheric boundary layers", *J. Wind Eng. Ind. Aerodyn.*, **79**, 11-35.

Florida Coastal Monitoring Program (2004), "Collected data: Frances", http://users.ce.ufl.edu/~fcmp/collected_data/storms/frances/towerdata.htm. Date accessed: 27 Feb. 2006.

Holmes, J. D. and Oliver, S. E. (2000), "An empirical model of a downburst", *Eng. Struct.*, **22**, 1167-1172.

Huston, D. R. (1986), *The Effects of Upstream Gusting on the Aeroelastic Behavior of Long Suspended-Span Bridges*, Princeton University Dissertation.

Kikitsu, H., Kanda, J., and Iwasaki, R. (1999), "Flow simulation by wind tunnel with computer-controlled multiple fans", *J. Wind Eng. Ind. Aerodyn.*, **83**, 421-429.

Kobayashi, H., Hatanaka, A., and Ueda, T. (1994), "Active simulation of time histories of strong wind gust in a wind tunnel", *J. Wind Eng. Ind. Aerodyn.*, **53**, 315-330.

Marshall, R. D. and Krayer, W. R. (1992), "Gust factors applied to hurricane winds", *Bull. American Meteorological Soc.*, **73**, 613-617.

Munson, B. R., Young, D. F., and Okiishi, T. H. (2002), *Fundamentals of Fluid Mechanics*, 4th Ed., John Wiley and Sons, Inc., New York.

Nishi, A., Kikugawa, H., Matsuda, Y., and Tashiro, D. (1999), "Active control of turbulence for an atmospheric boundary layer model in a wind tunnel", *J. Wind Eng. Ind. Aerodyn.*, **83**, 409-419.

Nishi, A. and Miyagi, H. (1995), "Computer-controlled wind-tunnel for wind-engineering applications", *J. Wind Eng. Ind. Aerodyn.*, **54/55**, 493-504.

Orwig-Gast, K. D. and Schroeder, J. L. (2005), "Extreme wind events observed in the 2002 thunderstorm

outflow experiment", *Proc. Tenth Americas Conference on Wind Engineering*, Baton Rouge, Louisiana.

Powell, M. D. and Houston, S. H. (1998), "Surface wind fields of 1995 hurricanes erin, opal, luis, marilyn, and roxanne at landfall", *Monthly Weather Review*, **126**, 1259-1273.

Rappaport, E. N. (1993), "Preliminary Report, Hurricane Andrew, 16-28 August, 1992", *National Hurricane Center*, National Weather Service, <http://www.nhc.noaa.gov/1992andrew.html>. Date accessed: 27 Feb. 2006.

Saric, W. S. (1992), "The ASU transition research facility", *AIAA 17th Aerospace Ground Testing Conference*, AIAA-92-3910.

Schroeder, J. L. and Smith, D. A. (1999), "Hurricane Bonnie wind flow characteristics as determined from WEMITE", *Wind Engineering into the 21st Century, Proc. of Tenth International Conference on Wind Engineering*, 329-335.

Sherman, D. J. (1987), "The passage of a weak-thunderstorm downburst over an instrumented tower", *Monthly Weather Review*, **115**, 1193-1205.

Simiu, E. and Scanlan, R. H. (1996), *Wind Effects on Structures*, 3rd Ed., John Wiley & Sons, Inc., New York, NY.

Wang, L. and Kareem, A. (2005), "Modeling and simulation of transient winds in downbursts/hurricanes", *Proc. 10th America's Conference on Wind Engineering*, Baton Rouge, Louisiana.

Appendix

This appendix describes the details of the loss coefficient calculations used to predict the bypass duct performance. Details are provided here concerning how the bypass duct loss coefficient, K_L^{BD}, was determined and how the test section circuit loss coefficients were estimated with respect to opening and closing the bypass duct.

The various parts of the bypass duct, as shown in Fig. 3, are modeled as individual components as shown in Fig. 5. Most of the loss coefficient expressions that were used in this model were derived originally for pipe flow but have been found to give reasonable results for ducts of various non-circular and rectangular cross section (Blevins 2003). Every component loss coefficient, referred to as $K_{L_i}^{BD}$, related to the bypass duct was referenced to V_{BD} so that they could be summed into a total bypass duct loss coefficient, K_L^{BD} (see the definition of K_L^{BD} in Eq. (4)). Similarly, loss coefficients related to the main wind tunnel circuit were all referenced to V_{WTopen} as required by the definition of K_L^{WTopen} in Eq. (5).

What follows is a description of each component loss coefficient in order. The exit and entrance flows were modeled as dividing and combining T's with loss coefficients given by Blevins (2003). The following expression applies to one leg of a dividing T, that is, for flow exiting from the main duct to the bypass duct as the following:

$$K_{L_i}^{BD} = \left[0.99 - 0.82\left(\frac{V_{slotopen1}}{V_{fanopen1}}\right) + 1.02\left(\frac{V_{slotopen1}}{V_{fanopen1}}\right)^2\right]\left(\frac{V_{fanopen1}}{V_{BDopen}}\right)^2 \qquad (9)$$

where $V_{fanopen1}$ is the velocity in the fan section downstream of the fan when the bypass duct dampers are open and $V_{slotopen1}$ is the average velocity through the exit slot connecting the main duct to the bypass duct. The ($V_{fanopen1}/V_{BD}$) factor references the loss coefficient to the bypass duct velocity. A slightly different expression was used for the entrance flow. It is important to note that the velocity, $V_{fanopen1}$, in the fan section downstream of the fan was estimated as an average velocity from the fan flow rate over an annular area between the duct wall (with a diameter of 2.74 m) and the fan hub (with a diameter of 1.27 m) and not as an average over the full duct diameter.

The loss coefficient for the bend in the plenum, $K_{L_2}^{BD}$, was modeled as a bend of given radius without turning vanes. This was found in Blevins (2003) to be 0.87. The loss coefficients for flow through a sudden contraction is dependent on the area ratio. The area of the plenum is larger than that of the bypass duct, and Blevins (2003) gives the following expression for the area contraction loss coefficient:

$$K_{L_3}^{BD} = \frac{1}{2}\left[1 - \frac{A_{BD}}{A_{p1}}\right] = 0.33 \tag{10}$$

where in this case A_{p1} is the area of one side of the plenum chamber downstream of the fan and A_{BD} is the area in one side of the smaller bypass duct. The area ratio is 0.34 which gives a loss coefficient of 0.33. This loss coefficient is referenced to the flow velocity in the A_{BD} section which is V_{BD}.

The loss coefficient for the damper vanes, $K_{L_4}^{BD}$, was found from the vendor-specified pressure drop through the vane array. This value was calculated to be 1.3 with respect to V_{BD}. The loss coefficient for flow through the narrow part of the duct itself, $K_{L_5}^{BD}$, was estimated as a typical duct flow using a hydraulic diameter of 1.55 m and a Moody chart (Blevins 2003). $K_{L_5}^{BD}$ was estimated to be 0.05.

$K_{L_6}^{BD}$ is the loss coefficient for an abrupt area expansion. From Blevins (2003), one finds:

$$K_{L_6}^{BD} = \left[1 - \frac{A_{BD}}{A_{p2}}\right] = 0.42 \tag{11}$$

where in this case A_{BD} is the area in the bypass duct and A_{p2} is the area in the plenum just upstream of the fan. This area ratio is 0.36, slightly larger than the contraction area ratio because the main duct has a slightly larger diameter upstream of the fan than downstream of the fan. This loss coefficient is given in terms of bypass duct velocity as well.

$K_{L_7}^{BD}$ is 0.87 from the second bend. The final component loss coefficient, $K_{L_8}^{BD}$, comes from an entrance flow, i.e., flow from the bypass duct reentering the main duct. Blevins (2003) gives the following expression for the appropriate leg of a combining T:

$$K_{L_8}^{BD} = \left[1.09 - 0.53\left(\frac{V_{WTopen2}}{V_{fanopen2}}\right) + 1.02\left(\frac{V_{WTopen2}}{V_{fanopen2}}\right)^2\right]\left(\frac{V_{fanopen2}}{V_{BDopen}}\right)^2 \tag{12}$$

where $V_{fanopen2}$ is the velocity in the fan section upstream of the fan when the bypass duct is open and $V_{WTopen2}$ is the velocity from the test section adjusted for the area past the entrance. The factor of $(V_{fanopen2}/V_{BD})$ references the loss coefficient to the bypass duct velocity. Similar to the case of the exit flow and $K_{L_1}^{BD}$, $V_{fanopen2}$ and $V_{WTopen2}$ were calculated from volume flow rates divided by annular areas between the duct wall (with a diameter of 2.84 m upstream of the fan) and the fan hub (with a diameter of 1.27 m).

Several of these contributions to the bypass duct loss coefficient are dependent on the flow rate through the fan section and through the bypass duct. As a result, the above expressions are part of the iterative procedure described in the text for finding the test section velocity when the bypass duct is open, V_{WTopen}. The values tabulated in for each component loss coefficient are those that were found as the velocity solution converged. The loss coefficient for the bypass duct, K_L^{BD}, was in this way estimated to be 15.2 with respect to the bypass duct velocity.

In addition to the K_L^{BD} estimate, an estimate was needed of the contributions of the open bypass duct slots and the damper orientation to the various main circuit loss coefficients, $K_L^{WT_{clean}}$, $K_L^{WT_{open}}$

and $K_L^{WT_{closed}}$.

The value of the clean tunnel (i.e. bypass slots covered) loss coefficient, $K_L^{WT_{clean}}$, had to be adjusted once the slots that connect the bypass duct to the main duct were uncovered. The two slot openings were modeled as pipe junctions with loss coefficients of 0.08 with respect to local velocity (Munson, *et al*. 2002). Referencing this loss coefficient value for the two slots to the test section velocity, $K_L^{WT_{open}}$, (as required by Eq. 5) resulted in an increased test section loss coefficient from a $K_L^{WT_{clean}}$ value of 0.64 to a $K_L^{WT_{closed}}$ value of 0.71.

The approach to estimate $K_L^{WT_{open}}$ started with the original, closed-duct loss coefficient ($K_L^{WT_{closed}}$) value of 0.71 and added contributions from dividing and combining T models similar to that used for K_L^{BD}. The loss coefficient for the non-exiting leg of a dividing T is given by Blevins (2003) as:

$$K_{L_{exit}}^{WT} = \left[1.55\left(0.22 - \frac{V_{slotopen1}}{V_{fanopen1}}\right)^2 - 0.13\right]\left(\frac{V_{fanopen1}}{V_{WTopen}}\right)^2 \tag{13}$$

where the $(V_{fanopen1} / V_{WTopen})$ factor references the loss coefficient to the test section velocity. The expression for the non-entering leg of a combining T is given by Blevins (2003) as:

$$K_{L_{entrance}}^{WT} = \left[0.045 + 1.38\frac{V_{slotopen2}}{V_{fanopen2}} - 0.90\left(\frac{V_{slotopen2}}{V_{fanopen2}}\right)\right]\left(\frac{V_{fanopen2}}{V_{WTopen}}\right)^2 \tag{14}$$

where $V_{slotopen2}$ is the average velocity through the entrance slot connecting the main duct to the bypass duct. Like the $K_{L_i}^{BD}$ values, the values for $K_{L_{exit}}^{WT}$ and $K_{L_{entrance}}^{WT}$ were dependent on the flow rate through the fan and had to be iteratively estimated along with the test section velocity V_{WTopen}. These values were added to 0.71 to arrive at an estimate for $K_L^{WT_{open}}$ of 1.07.

CC